Research Article

Hybrid Analytical and MLS-Based NMM for the Determination of Generalized Stress Intensity Factors

Feng Liu,[1] Hong Zheng,[2] and Xiuli Du[2]

[1]*State Key Laboratory of Geomechanics and Geotechnical Engineering, Institute of Rock and Soil Mechanics, Chinese Academy of Sciences, Wuhan 430071, China*
[2]*Key Laboratory of Urban Security and Disaster Engineering, Ministry of Education, Beijing University of Technology, Beijing 100124, China*

Correspondence should be addressed to Hong Zheng; hzheng@whrsm.ac.cn

The numerical manifold method (NMM) is characterized by its two cover systems, the mathematical cover and the physical cover. In the standard NMM, the mathematical cover is required to cover the whole problem domain. In this study, however, around each crack tip we specify a small domain on which the displacement is taken as the truncated Williams' displacement series. And accordingly all such small domains are not covered by the mathematical cover that only covers the rest of the problem domain. Meanwhile, the mathematical cover is constructed by designating all supports of the scattered nodes arising in the moving least squares interpolation as the mathematical patches. In this way, any physical patch contains no crack tip and can be approximated by polynomials. As a result, no blending element issue exists as in the extended finite element method and NMM. In addition to high precision, the proposed procedure is especially suitable for the situation where a crack tip is very close to other cracks, a case difficult to treat by the interaction integral procedure that is commonly used in the extraction of the stress intensity factors of mixed mode cracks.

1. Introduction

The extended finite element method (XFEM [1, 2]) was first introduced by Belytschko and Black and Moës et al. in 1999. The main idea of XFEM is to superpose enriched terms to the classical finite element approximation. The crack is represented independently of the mesh, allowing for simulation of the crack propagation without remeshing. It is known that the convergence rate of XFEM is influenced by the transition layer between the singular enrichment area and the rest of the domain. Some strategies for improving the convergence rate of XFEM can be found in [3–5]. Another effective approach to model crack problems is the numerical manifold method (NMM [6–14]). Besides XFEM and NMM, there are some other related methods, such as mesh-free method [15–18], cracking particles method [19], extended isogeometric analysis (XIGA [20]), and immersed particles method [21].

Usually, neither XFEM nor NMM directly estimates the stress intensity factors (SIFs). Instead, they utilize a postprocessing procedure, called the interaction integral procedure [2], to extract SIFs of a mixed mode crack. If the crack is very close to another crack, however, the interaction integral procedure cannot work very well because a local domain containing the crack tip, selected for the calculation of the J integral, might be cut by the neighboring crack unless the local domain is selected very small. But if the local domain is too small, the precision of the resulting SIFs is compromised considerably.

To solve the above issue, some special techniques have been developed to conduct the crack analysis, where the SIFs are selected as the basic unknowns and can be solved directly. Liu et al. [22] enriched the approximation surrounding the crack tip with the truncated Williams' series and force the enriched DOFs to be equal. The enriched DOFs are actually

the generalized SIFs. The numerical experiences indicate that this approach does not always reach high precision since the blending elements are still present.

Réthoré et al. [23] developed a hybrid analytical and extended finite element method, abbreviated as HAX-FEM. By HAX-FEM, the problem domain Ω is subdivided into two overlapping subdomains Ω_W and Ω_X. Here, Ω_W is a small domain around the crack tip and, for the simplicity in presentation, Ω is assumed to contain only one crack tip. On Ω_W the displacement is expressed by a truncated Williams' series, while the displacement on Ω_X is approximated by the conventional XFEM. Due to the presence of the overlapping subdomain, the energy coupling procedure was utilized in the weak formulation so as not to commit the variational crime. In order not to avoid the overlapping subdomain, another artificial thing, Passieux et al. [24] proposed that Ω_W and Ω_X do not overlap, and the displacement continuity across the interface between Ω_W and Ω_X is enforced by the Lagrange multiplier method, which will lead to an indefinite system of linear equations. And the approximation to the Lagrange multiplier is not so easy such that the LBB condition is satisfied. To avoid the introduction of the Lagrange multiplier, recently Zhuang et al. [25] suggested that in Ω_W the stress is taken as the basic field variable instead of the displacement, where the weak formulation is derived from the mixed energy functional proposed by Long and Zhao [26]. This procedure is able to achieve an accurate evaluation of SIFs, but the displacement in Ω_W is hard to calculate accurately. The open degree of cracks is important for the situations such as the exploitation of shale gas by the hydraulic fracture technique.

In this study, the MLS-based NMM is used to evaluate directly the SIFs of mixed mode cracks. The MLS-based NMM enjoys the merits owned by the element-free Galerkin (EFG [15]) method and the NMM [6], which has been verified in the analysis of free boundary value problems such as the unconfined seepage analysis [27], and will be further confirmed by the challenging examples on crack analysis in the sequel.

2. Elastic Crack Tip Asymptotic Fields

The crack tip asymptotic fields, including displacement and stress fields, of a plane crack in a linear elastic brittle material with traction-free faces can be expressed in the so-called Williams' expansions [28]. If the crack lies on the negative x-axis and the polar coordinates centered at the crack tip are designated r and θ (counterclockwise from the positive x-axis), Williams' series (truncated to N terms) for the displacement can be written as

$$
u_x = \sum_{n=0}^{N} \frac{r^{n/2}}{2\mu} \left\{ A_n \left[\left(\kappa + \frac{n}{2} + (-1)^n \right) \cos \frac{n}{2}\theta \right. \right.
$$
$$
\left. - \frac{n}{2} \cos \left(\frac{n}{2} - 2 \right) \theta \right]
$$
$$
\left. - B_n \left[\left(\kappa + \frac{n}{2} - (-1)^n \right) \sin \frac{n}{2}\theta \right. \right.
$$
$$
\left. \left. - \frac{n}{2} \sin \left(\frac{n}{2} - 2 \right) \theta \right] \right\},
$$

$$
u_y = \sum_{n=0}^{N} \frac{r^{n/2}}{2\mu} \left\{ A_n \left[\left(\kappa - \frac{n}{2} - (-1)^n \right) \sin \frac{n}{2}\theta \right. \right.
$$
$$
\left. + \frac{n}{2} \sin \left(\frac{n}{2} - 2 \right) \theta \right]
$$
$$
+ B_n \left[\left(\kappa - \frac{n}{2} + (-1)^n \right) \cos \frac{n}{2}\theta \right.
$$
$$
\left. \left. + \frac{n}{2} \cos \left(\frac{n}{2} - 2 \right) \theta \right] \right\},
$$
$$
\tag{1}
$$

where $\mu = E/(2(1+\nu))$ is the shear modulus; the Kolosov constant κ is equal to $(3-\nu)/(1+\nu)$ for plane stress and $3-4\nu$ for plane strain conditions; E and ν are Young's modulus and Poisson's ratio. The terms containing A_n and B_n are related to the mode I and mode II parts of deformation, respectively. Here is a brief review of some notable properties of this expansion. The rigid body translation of the crack depends on the coefficients A_0 and B_0 and the rigid body rotation with respect to the crack tip depends on B_2. The second term in the mode I expansion is often referred to as the elastic T-stress component. The coefficients A_1 and B_1 are related to the mode I and mode II stress intensity factors (SIFs) as

$$
A_1 = \frac{K_{\mathrm{I}}}{\sqrt{2\pi}}, \qquad B_1 = -\frac{K_{\mathrm{II}}}{\sqrt{2\pi}}. \tag{2}
$$

Traditionally, the SIFs are important for the determination of the initiation and propagation of cracks in brittle materials. However, some recent studies show that higher-order terms of the asymptotic field are of great relevance for predicting the constraint of elastoplastic crack tip fields [29] and for interpreting the size effect of quasi-brittle materials. So evaluating the higher-order terms of Williams' expansions, called generalized stress intensity factors together with the conventional SIFs, is also necessary.

3. Problem Formulation

Let us consider the elastic body with a traction-free crack surface Γ_c shown in Figure 1 (reproduced from [24]). The prescribed displacement $\overline{\mathbf{u}}$ is imposed on Γ_u, while traction t_0 is acted on Γ_t. The domain is divided into two nonoverlapping subdomains Ω_X and Ω_W with unknown displacements $\mathbf{u}_X$ and $\mathbf{u}_W$, respectively. In domain Ω_X, the approximation of displacement $\mathbf{u}_X$ is described by the MLS-based NMM, which will be discussed in the next section. In domain Ω_W, we approximate the displacement by the truncated Williams' series given by (1).

In [24], the displacement continuity across the interface Γ_W is enforced by the Lagrange multiplier method. As the number of crack tips increases, the number of Lagrange multipliers will increase rapidly. So the penalty method is adopted in this study. In fact, the results created by the two methods are very small due to the numerical excellence of
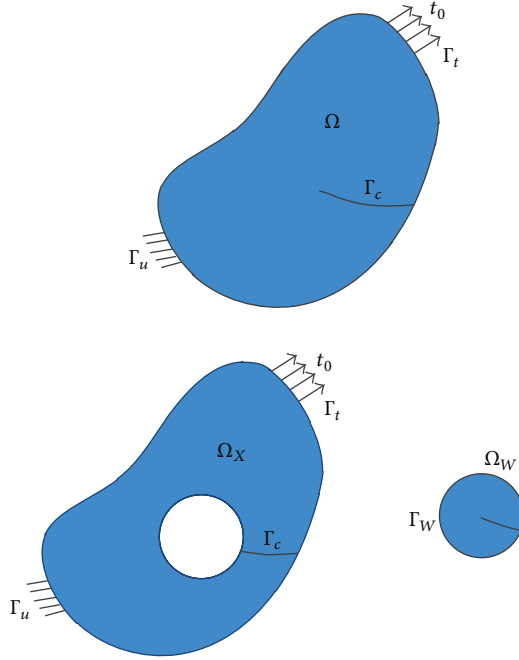
FIGURE 1: Decomposition of the domain into a standard domain and an analytical patch.

FIGURE 2: A crack cuts one mathematical patch into two physical patches.

NMM; see [30], for example. In this way, we construct the conventional potential as follows:

$$
\begin{aligned}
\pi\left(\mathbf{u}_X, \mathbf{u}_W\right) = & \int_{\Omega_X} \frac{1}{2} \boldsymbol{\varepsilon}\left(\mathbf{u}_X\right)^T \mathbf{D} \boldsymbol{\varepsilon}\left(\mathbf{u}_X\right) d\Omega \\
& + \int_{\Omega_W} \frac{1}{2} \boldsymbol{\varepsilon}\left(\mathbf{u}_W\right)^T \mathbf{D} \boldsymbol{\varepsilon}\left(\mathbf{u}_W\right) d\Omega \\
& + \int_{\Gamma_W} \frac{1}{2} k_p \left(\mathbf{u}_X - \mathbf{u}_W\right)^2 d\Gamma - \int_{\Gamma_t} \mathbf{u}_X{}^T \mathbf{t}_0 \, d\Gamma \\
& + \int_{\Gamma_u} \lambda^T \left(\mathbf{u}_X - \overline{\mathbf{u}}\right) d\Gamma,
\end{aligned}
\tag{3}
$$

where $\boldsymbol{\varepsilon}$ is the infinitesimal strain tensor, $\mathbf{D}$ is elastic matrix, Γ_W is the interface between Ω_X and Ω_W, k_p is the penalty factor, and λ is the Lagrange multiplier associated with the essential boundary condition. We assume that the boundary conditions are held by Ω_X only since Ω_W is a quite small domain around the crack tip. The equation can be extended to multiple crack tips problem straightly.

3.1. Standard Subdomain. In domain Ω_X, MLS-based NMM is used to approximate the displacement. The salient feature of NMM is the introduction of two covers, namely, the mathematical cover (MC) and the physical cover (PC). The MC consists of mathematical patches (MP), each of which is a rectangle or hexagon usually. The MCs do not need to match the boundary of the domain, as long as they cover the whole domain. The construction of physical patches is accomplished by cutting the mathematical patches using discontinuity lines, such as cracks and material boundaries. All the physical
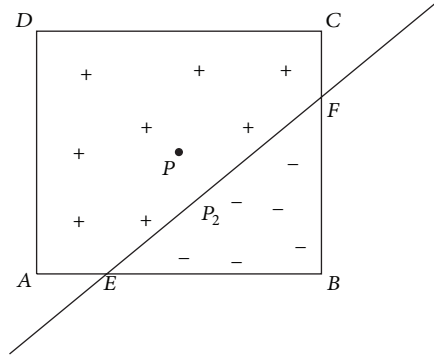
patches form the PC covering exactly the problem domain. The main purpose to introduce two covers is to solve in a unified way the continuum and discontinuum problems. Moreover, the best approximation to the primal field variables can be guaranteed because we can always use a uniform mesh to construct the MC.

Here, we give a brief illustration on how NMM simulates the discontinuity. First, we deploy over Ω_X some nodes. Unlike EFG, all these nodes, called mathematical nodes, can be allowed to be outside Ω_X, as long as their influence domains have intersection with Ω_X. All the influence domains of these mathematical nodes constitute the MC covering Ω_X. Let us cut the mathematical patch of node P (denoted as quadrilateral ABCD) by a crack (the bold line) into 2 patches: pentagon AEFCD and triangle EBF, respectively, as shown in Figure 2. Both of the two patches are physical patches of the PC in construction. We add a new physical node, denoted by P_2, and associate P_2 with triangle EBF. At this moment, P_2 has the same coordinate as P. The degrees of freedom associated with the two physical nodes P and P_2 are separate, reproducing strong discontinuity along the crack. So, in NMM, there is no need to introduce the Heaviside enrichment function which is widely used in XFEM. Details can be found in [9, 12].

For zero-order NMM, which is used in this paper, the displacement interpolation can be expressed as

$$
\mathbf{u}_X(x) = \sum_{i \in N_P} N_i(x) u_i(x) = \mathbf{N}_X \mathbf{U}_X,
\tag{4}
$$

where N_P is the set of all physical nodes, u_i is the degree of freedom, and $N_i(x)$ is the corresponding shape function with both associated with node-i. Here, we use the MLS shape function with linear basis and rectangular influence domain instead of the FEM shape function. The MLS interpolation is discussed in detail in [15, 31].

3.2. Analytical Patch. On domain Ω_W, the displacement is described by the truncated Williams' series (1) only. So no mesh is needed theoretically. Rewrite (1) as

$$
\mathbf{u}_W(x) = \begin{bmatrix} u_x \\ u_y \end{bmatrix} = \sum_{n=0}^{N} \frac{r^{n/2}}{2\mu} \begin{bmatrix} f_1 & f_2 \\ f_3 & f_4 \end{bmatrix} \begin{bmatrix} A_n \\ B_n \end{bmatrix} = \mathbf{N}_W \mathbf{U}_W,
\tag{5}
$$

where N is the maximum order of the truncated Williams' series; f_1, f_2, f_3, and f_4 are extracted from (1). Since the SIFs and higher-order terms are related to special A_n and B_n above, generalized stress intensity factors can be evaluated directly.

3.3. Matching Interface. The third term on the right of (3) stands for the matching of standard subdomain and analytical patch. No more unknowns are introduced through penalty method.

3.4. System of Equations. Though no mesh is needed for MLS interpolation, a background mesh is essential for numerical integration. In practice, a circle of radius $R_W = hr_W$ centered at the crack tip is defined first. Here, h is the average element size of the mesh and r_W is a dimensionless size controlling the region of Ω_W. All the elements in or in intersection with the circle constitute subdomain Ω_W, while the rest constitute subdomain Ω_X. The outer boundary of Ω_W, which equals the inner boundary of Ω_X, is the common interface Γ_W.

Putting $\delta\pi(\mathbf{u}_X, \mathbf{u}_W) = 0$ and replacing $\mathbf{u}_X(x)$ and $\mathbf{u}_W(x)$ by (4) and (5), we have the equations system as follows:

$$\begin{bmatrix} \mathbf{K}_X + \mathbf{H}_X & \mathbf{L}^T & \mathbf{G}^T \\ \mathbf{L} & \mathbf{K}_W + \mathbf{H}_W & 0 \\ \mathbf{G} & 0 & 0 \end{bmatrix} \begin{bmatrix} \mathbf{u} \\ \mathbf{a} \\ \mathbf{\Lambda} \end{bmatrix} = \begin{bmatrix} \mathbf{P} \\ 0 \\ \mathbf{Q} \end{bmatrix}, \quad (6)$$

where

$$\mathbf{K}_X = \int_{\Omega_X} \mathbf{B}_X^T \mathbf{D} \mathbf{B}_X \, d\Omega, \qquad \mathbf{K}_W = \int_{\Omega_W} \mathbf{B}_W^T \mathbf{D} \mathbf{B}_W \, d\Omega,$$

$$\mathbf{H}_X = \int_{\Gamma_X} \mathbf{N}_X^T \mathbf{N}_X \, d\Omega, \qquad \mathbf{H}_W = \int_{\Gamma_W} \mathbf{N}_W^T \mathbf{N}_W \, d\Omega,$$

$$\mathbf{L} = \int_{\Gamma_X} \mathbf{N}_W^T \mathbf{N}_X \, d\Omega, \qquad \mathbf{G} = \int_{\Gamma_u} \mathbf{N}_\lambda^T \mathbf{N}_X \, d\Omega, \qquad (7)$$

$$\mathbf{P} = \int_{\Gamma_t} \mathbf{N}_X^T \mathbf{t}_0 \, d\Omega, \qquad \mathbf{Q} = \int_{\Gamma_u} \mathbf{N}_\lambda^T \overline{\mathbf{u}} \, d\Omega.$$

$\mathbf{u}$ is the degrees of freedom in domain Ω_X, $\mathbf{a}$ is the degrees of freedom in domain Ω_W, and $\mathbf{\Lambda}$ is the Lagrange multipliers associated with Γ_u.

To obtain $\mathbf{B}_X$ and $\mathbf{B}_W$, we should utilize the compatibility equation:

$$\varepsilon_{ij} = \frac{1}{2}\left(\frac{\partial u_i}{\partial x_j} + \frac{\partial u_j}{\partial x_i}\right). \quad (8)$$

Substituting (4) into (8) and comparing the result with equation $\boldsymbol{\varepsilon}_X(x) = \mathbf{B}_X\mathbf{U}_X$, matrix $\mathbf{B}_X$ is obtained. We can derive $\mathbf{B}_W$ in a similar way.

The background mesh is used for integrating the matrices in (6). For the elements cut by no discontinuity, 4×4 Gauss's points are used. For the elements cut by cracks or boundaries they are subdivided into a set of triangles and each triangle integrated by 13-point Hammer integration. For the element with a crack tip inside, a special technique [12] is used to eliminate the singularity.
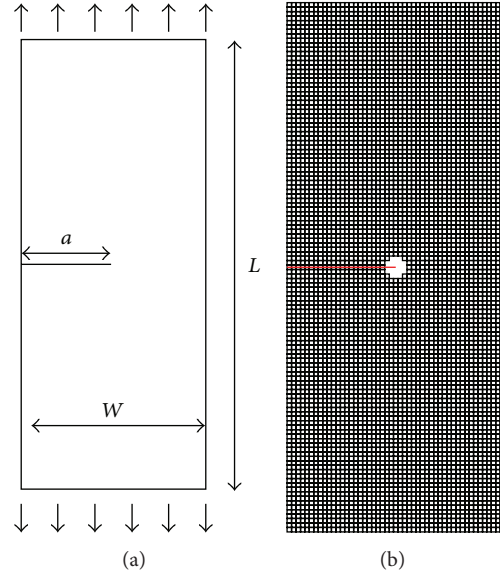

(a)   (b)

Figure 3: Edge-cracked plate under remote tension: (a) geometry and loading; (b) mesh and patch for $r_W = 2$.

4. Numerical Examples

Several examples are studied to show the efficiency of the proposed method. The first one is an edge-cracked plate under remote tension. The choice of truncated order and the convergence are investigated. Secondly the centre-cracked plate under uniaxial tension (CCPT) and pure shearing (CCPS) are used to evaluate the generalized stress intensity factors. At last a star crack is provided to show the excellent performance of proposed method for complex cracks. In all these examples, the rectangular weight function with double node spacing is adopted.

4.1. Edge-Cracked Plate under Remote Tension. The edge-cracked plate considered here is shown in Figure 3(a). To compare with [24], the parameters are as follows: $L = 17$ mm, $W = 7$ mm, $a = 3.5$ mm, Poisson's ratio $v = 0.3$, and Young's modulus $E = 200$ GPa. A state of plane stress condition is assumed.

A uniform mesh of 49×119 elements is used. The mesh, the patch (with $r_W = 2$), and the crack (the red line) are plotted in Figure 3(b). The reference solution [24] of K_I for this problem is $K_{I0} = 2.9637$ MPa $\sqrt{m}$.

The normalized value of K_I is plotted as a function of the dimensionless size r_W in Figure 4 with different orders N of truncated Williams' expansion. A similar tendency is observed as in [24]. The dependence on the dimensionless size r_W vanishes when N is higher than 2. For the same N, the precision decreases as the size r_W increases, indicating that the analytical patch only influences near the crack tip. Since the influence domain of nodes in MLS is larger than that of XFEM, $r_W = 1$ leads to a wrong solution. For general case, $r_W = 2$ or $r_W = 3$ is recommended and used in the following examples.
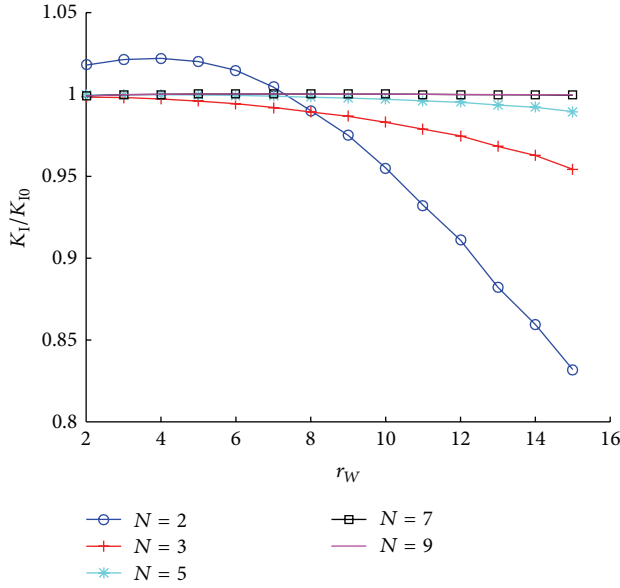
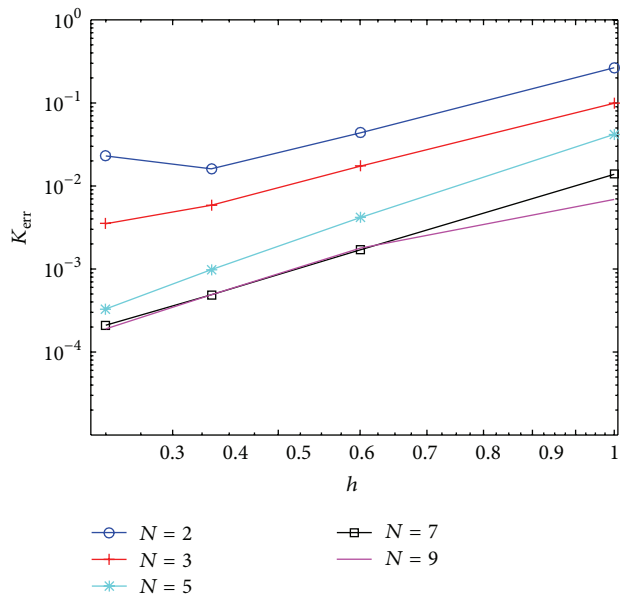FIGURE 4: Normalized K_I as function of the size of the patch for different values of N.

FIGURE 5: Relative error of K_I as function of node spacing for different values of N.

To consider the convergence of proposed method, the relative error of K_I is plotted as a function of the mesh size h in Figure 5 with different orders N of truncated Williams' series. The relative error of K_I is defined as

$$K_{err} = \frac{|K_I - K_{I0}|}{K_{I0}}. \tag{9}$$

The convergence rates of relative error of K_I are around 2, larger than the value 1.25 to 1.5 in [24]. By the convergence rate we mean the average slope of $\log(K_{err})/\log(h)$. Again we can see that when N is above 2, accurate SIFs can be obtained.
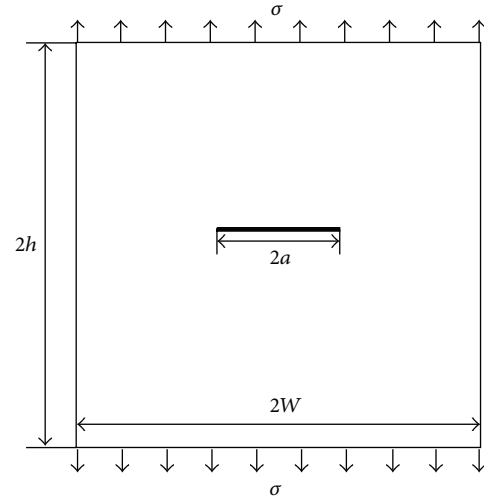

(a)
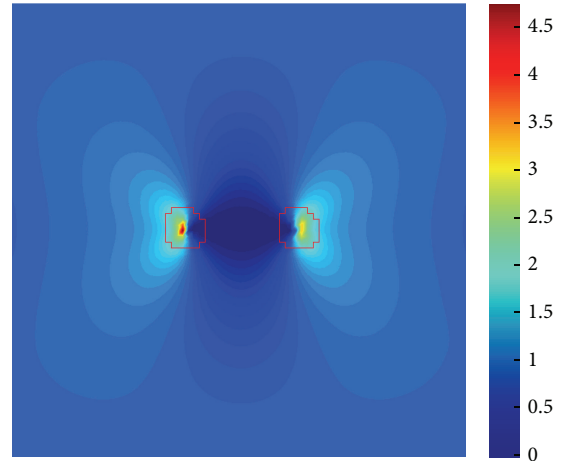
(b)

FIGURE 6: The CCPT specimen: (a) geometry and loading; (b) σ_y-stress nephogram for $r_W = 3$.

For the range of penalty factor in $10^3 \sim 10^5 E$, almost the same results are generated.

4.2. A Centre-Cracked Plate under Uniaxial Tension or Pure Shearing.

The centre-cracked plate under uniaxial tension (CCPT) is selected to investigate the pure mode I crack parameters (Figure 6(a)). In order to compare the results with the reference, the following geometry and loading parameters are used: $W = h = 4$, $\sigma = 1$, and crack length $a = 2$. A 80×80 mesh is used. In this case, $N = 14$ together with $r_W = 3$ are used to calculate the coefficients of Williams' expansion. The penalty factor is assumed to be $1000E$. Figure 6(b) shows the σ_y-stress nephogram, where the red lines represent the common interface of Ω_X and Ω_W. Table 1 shows the coefficients $A_1 - A_5$, B_1, and $B_3 - B_5$ for CCPT specimens in comparison with the results provided by other researchers [32, 33]. It seems that the results here are in good agreement with the results of finite element overdeterministic (FEOD

TABLE 1: Coefficients A_1–A_5, B_1, and B_3–B_5 for CCPT specimens ($a/W = 0.25$).

	A_1	B_1	A_2	A_3	B_3	A_4	B_4	A_5	B_5
Present	0.7674	−0.0002	−0.2761	0.1830	0.0001	0.0026	0.0001	−0.0235	−0.0003
FEOD	0.7679	0.0000	−0.2778	0.1866	0.0000	0.0030	−0.0001	−0.0275	−0.0000
HCE	0.7665	—	−0.2779	0.1915	—	−0.0018	—	−0.0235	—
BCM	0.7680	—	−0.2777	0.1866	—	0.0030	—	−0.0279	—
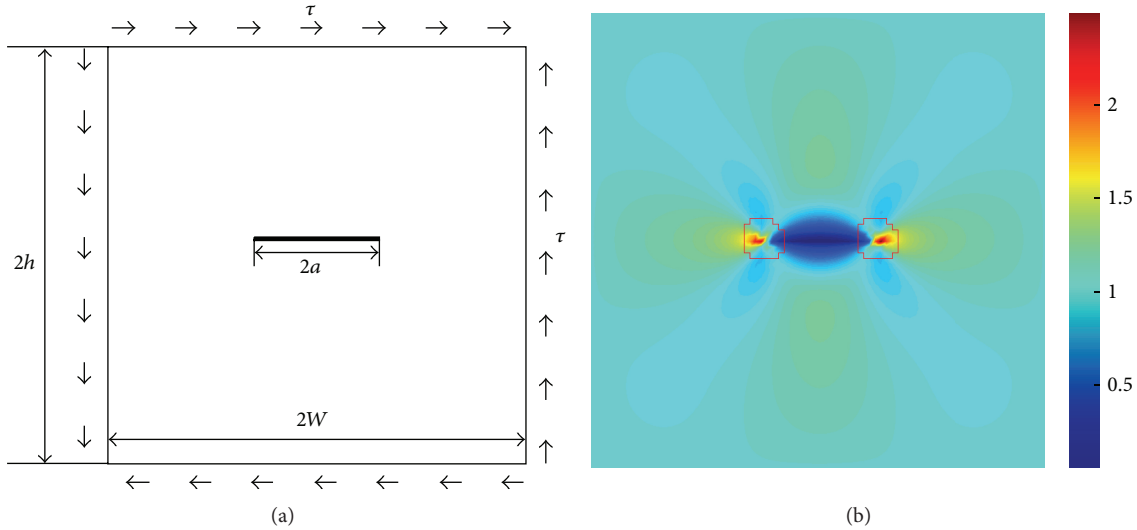
FIGURE 7: The CCPS specimen: (a) geometry and loading; (b) τ_{xy}-stress nephogram for $r_W = 3$.

[21]) method. Only A_1–A_5 are given for hybrid crack element (HCE) and boundary collocation method (BCM) in [32]. In fact, the results of HCE in Table 1 are calculated by half-crack model with only mode I considered. HCE considering half-crack model with mixed mode leads to wrong results for the coefficients of higher-order parameters.

Now consider the centre-cracked plate under pure shearing (CCPS). It is a typical example of mode II. The geometrical parameters of the CCPS (Figure 7(a)), the mesh, and material properties are the same as CCPT. Here, a uniformly distributed shear force $\tau = 1$ is imposed. Figure 7(b) gives the τ_{xy}-stress nephogram and again the red lines represent the interfaces. The coefficients A_1–A_5, B_1, and B_3–B_5 are shown in Table 2. Good agreement is observed between the present results and those of FEOD, HCE, and BCM. Again results of HCE in Table 2 are calculated by half-crack model with only mode II considered.

Both of these two examples illustrate that the present method can predict the generalized stress intensity factors precisely. No special treatment is needed throughout the whole process.

4.3. A Star-Shaped Crack in a Square Plate.
At last a star-shaped crack is analyzed which is often viewed as a representation of complex cracks. The star-shaped crack in a square plate subjected to biaxial tension is shown in Figure 8.

The normalized stress intensity factors at tips A and B are defined as

$$F_I^A = \frac{K_I^A}{\sigma\sqrt{\pi a}}, \qquad F_I^B = \frac{K_I^B}{\sigma\sqrt{\pi a}}, \qquad F_{II}^B = \frac{K_{II}^B}{\sigma\sqrt{\pi a}}. \qquad (10)$$

In this example, the plate dimension is fixed to be $W = 5$, and material constants are Young's modulus $E = 200000$ and Poisson's ratio $\nu = 0.3$. The biaxial tension σ is taken to be unity. The influence of the finiteness of plate on the SIFs is also investigated. Since the mesh refinement with no limit is one of the major advantages for MLS interpolation, hierarchical meshes are used around every crack tip here. The mesh (with 4 layers of hierarchical meshes near the tip) and detailed view with analytical patches are plotted in Figure 9 with $a/W = 0.1$. The cracks are moved with a small distance to avoid special case caused by symmetry. Here $N = 5$ and $r_W = 3$ are selected. The computed SIF results are summarized and compared with three reference solutions, respectively, from Cheung et al. [34], Daux et al. [35], and Ma et al. [7] in Table 3. From this table, good agreement can be easily seen. This example also shows that the proposed method can implement local refinement and handle complex crack straightly.

5. Conclusions

A hybrid analytical and numerical manifold method is proposed to analyze crack problems. The analytical subdomain

TABLE 2: Coefficients A_1–A_5, B_1, and B_3–B_5 for CCPS specimens ($a/W = 0.25$).

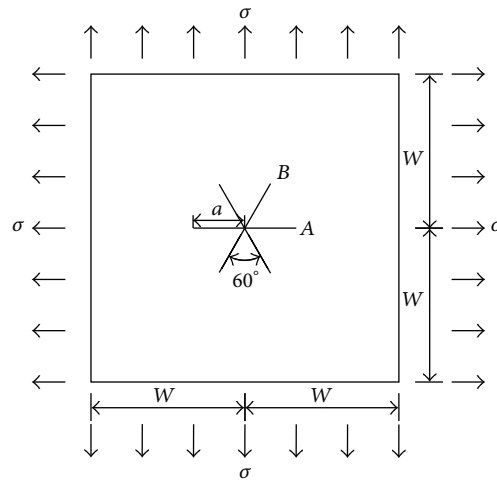|	A_1	B_1	A_2	A_3	B_3	A_4	B_4	A_5	B_5
Present	−0.0002	−0.7422	0.0000	0.0005	−0.1848	−0.0009	−0.0047	−0.0002	0.0264
FEOD	0.0010	−0.7403	−0.0011	0.0011	−0.1840	−0.0003	−0.0024	−0.0000	0.0234
HCE	—	−0.7414	—	—	−0.1835	—	−0.0045	—	0.0270
BCM	—	−0.7422	—	—	−0.1841	—	−0.0034	—	0.0242

FIGURE 8: A star-shaped crack in a square plate under biaxial tension.
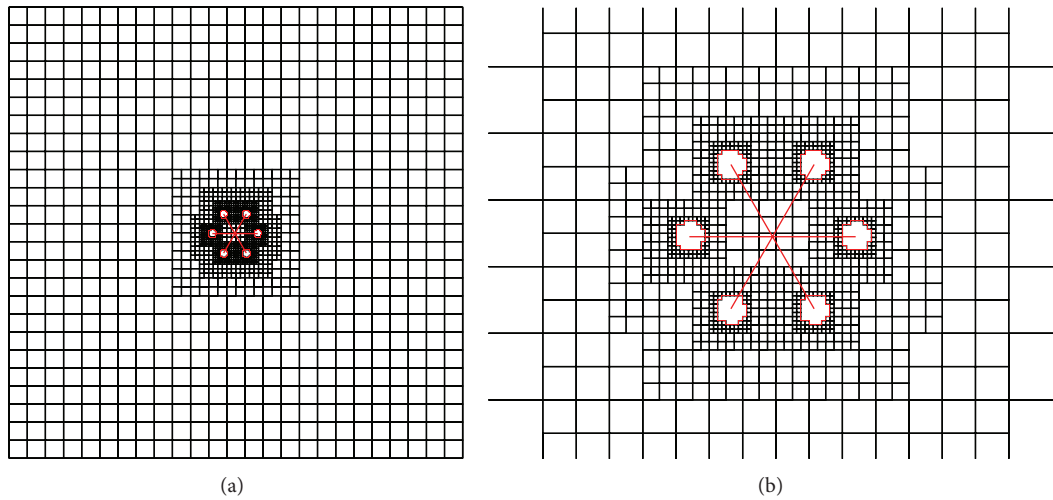

(a)

(b)

FIGURE 9: Star-shaped crack and the hierarchical meshes: (a) global view; (b) local view with analytical patches.

near the crack tip is described by the truncated Williams' expansions and the rest is modeled by the MLS-based NMM. Then, the two parts are coupled by the penalty method. The variational formulation and discrete equations are carefully discussed. The introduction of the analytical patch is to directly determine generalized stress intensity factors, while the advantage of MLS-based NMM is the simplicity in dealing with complex cracks and local refinement. The numerical experiments show that the proposed method is a promising approach for crack problems.

Conflict of Interests

The authors declare that there is no conflict of interests regarding the publication of this paper.

TABLE 3: Normalized SIFs comparison for a star-shaped crack.

a/W	F_I^A				F_I^B				F_{II}^B			
	T	$*$	$**$	$***$	T	$*$	$**$	$***$	T	$*$	$**$	$***$
0.1	0.7447	0.7408	0.7511	0.758	0.7463	0.7408	0.7690	0.767	−0.0003	0.0000	0.0001	0.000
0.2	0.7629	0.7570	0.7670	0.771	0.7649	0.757	0.7683	0.771	0.0005	0.0004	0.0005	0.000
0.3	0.7913	0.7846	0.7931	0.789	0.7961	0.7884	0.7983	0.798	0.0018	0.0022	0.0021	0.002
0.4	0.8319	0.8255	0.8287	0.821	0.8470	0.8365	0.8466	0.854	0.0074	0.0070	0.0080	0.007
0.5	0.8887	0.8815	0.8864	0.887	0.9229	0.9087	0.9255	0.924	0.0186	0.0168	0.0184	0.016
0.6	0.9712	0.9758	0.9673	0.971	1.0404	1.0182	1.0445	1.040	0.0355	0.0338	0.0364	0.036
0.7	1.1035	1.1142	1.0971	1.107	1.2334	1.1936	1.2367	1.234	0.0600	0.0529	0.0593	0.061
0.8	1.3398	—	1.3423	1.340	1.5631	—	1.5624	1.559	0.0847	—	0.0864	0.082
0.9	1.8801	—	1.9037	1.930	2.1968	—	2.1927	2.166	0.0870	—	0.0868	0.089

"—" means no corresponding solution.
*Cheung et al. (1992) [34]; **Daux et al. (2000) [35]; ***Ma et al. (2009) [7].

Acknowledgments

References

[1] T. Belytschko and T. Black, "Elastic crack growth in finite elements with minimal remeshing," *International Journal for Numerical Methods in Engineering*, vol. 45, no. 5, pp. 601–620, 1999.

[2] N. Moës, J. Dolbow, and T. Belytschko, "A finite element method for crack growth without remeshing," *International Journal for Numerical Methods in Engineering*, vol. 46, no. 1, pp. 131–150, 1999.

[3] E. Béchet, H. Minnebo, N. Moës, and B. Burgardt, "Improved implementation and robustness study of the X-FEM for stress analysis around cracks," *International Journal for Numerical Methods in Engineering*, vol. 64, no. 8, pp. 1033–1056, 2005.

[4] P. Laborde, J. Pommier, Y. Renard, and M. Salaün, "High-order extended finite element method for cracked domains," *International Journal for Numerical Methods in Engineering*, vol. 64, no. 3, pp. 354–381, 2005.

[5] E. Chahine, P. Laborde, and Y. Renard, "A non-conformal eXtended finite element approach: integral matching XFEm," *Applied Numerical Mathematics*, vol. 61, no. 3, pp. 322–343, 2011.

[6] G. H. Shi, "Manifold method of material analysis," DTIC Document, 1991.

[7] G. W. Ma, X. M. An, H. H. Zhang, and L. X. Li, "Modeling complex crack problems using the numerical manifold method," *International Journal of Fracture*, vol. 156, no. 1, pp. 21–35, 2009.

[8] G. Zhang, Y. Zhao, and X. Peng, "Simulation of toppling failure of rock slope by numerical manifold method," *International Journal of Computational Methods*, vol. 7, no. 1, pp. 167–189, 2010.

[9] X. An, G. Fu, and G. Ma, "A comparison between the nmm and the XFEM in discontinuity modeling," *International Journal of Computational Methods*, vol. 9, no. 2, Article ID 1240030, 2012.

[10] Z. Wu and L. N. Y. Wong, "Frictional crack initiation and propagation analysis using the numerical manifold method," *Computers and Geotechnics*, vol. 39, pp. 38–53, 2012.

[11] H. H. Zhang, "Analysis of crack interaction problem by the numerical manifold method," *Advanced Materials Research*, vol. 446–449, pp. 797–801, 2012.

[12] H. Zheng and D. Xu, "New strategies for some issues of numerical manifold method in simulation of crack propagation," *International Journal for Numerical Methods in Engineering*, vol. 97, no. 13, pp. 986–1010, 2014.

[13] G. Ma, X. An, and L. He, "The numerical manifold method: a review," *International Journal of Computational Methods*, vol. 7, no. 1, pp. 1–32, 2010.

[14] H. Zheng, F. Liu, and C. Li, "The MLS-based numerical manifold method with applications to crack analysis," *International Journal of Fracture*, vol. 190, no. 1-2, pp. 147–166, 2014.

[15] T. Belytschko, Y. Y. Lu, and L. Gu, "Element-free Galerkin methods," *International Journal for Numerical Methods in Engineering*, vol. 37, no. 2, pp. 229–256, 1994.

[16] G. Ventura, J. X. Xu, and T. Belytschko, "A vector level set method and new discontinuity approximations for crack growth by EFG," *International Journal for Numerical Methods in Engineering*, vol. 54, no. 6, pp. 923–944, 2002.

[17] X. Zhuang, C. Augarde, and S. Bordas, "Accurate fracture modelling using meshless methods, the visibility criterion and level sets: formulation and 2D modelling," *International Journal for Numerical Methods in Engineering*, vol. 86, no. 2, pp. 249–268, 2011.

[18] M. Fleming, Y. A. Chu, B. Moran, T. Belytschko, Y. Lu, and L. Gu, "Enriched element-free Galerkin methods for crack tip fields," *International Journal for Numerical Methods in Engineering*, vol. 40, no. 8, pp. 1483–1504, 1997.

[19] T. Rabczuk and T. Belytschko, "Cracking particles: a simplified meshfree method for arbitrary evolving cracks," *International Journal for Numerical Methods in Engineering*, vol. 61, no. 13, pp. 2316–2343, 2004.

[20] S. S. Ghorashi, N. Valizadeh, and S. Mohammadi, "Extended isogeometric analysis for simulation of stationary and propagating cracks," *International Journal for Numerical Methods in Engineering*, vol. 89, no. 9, pp. 1069–1101, 2012.

[21] T. Rabczuk, R. Gracie, J.-H. Song, and T. Belytschko, "Immersed particle method for fluid-structure interaction," *International Journal for Numerical Methods in Engineering*, vol. 81, no. 1, pp. 48–71, 2010.

[22] X. Y. Liu, Q. Z. Xiao, and B. L. Karihaloo, "XFEM for direct evaluation of mixed mode SIFs in homogeneous and bi-materials,"

International Journal for Numerical Methods in Engineering, vol. 59, no. 8, pp. 1103–1118, 2004.

[23] J. Réthoré, S. Roux, and F. Hild, "Hybrid analytical and extended finite element method (HAX-FEM): a new enrichment procedure for cracked solids," *International Journal for Numerical Methods in Engineering*, vol. 81, no. 3, pp. 269–285, 2010.

[24] J. C. Passieux, A. Gravouil, J. Réthoré, and M. C. Baietto, "Direct estimation of generalized stress intensity factors using a three-scale concurrent multigrid X-FEM," *International Journal for Numerical Methods in Engineering*, vol. 85, no. 13, pp. 1648–1666, 2011.

[25] X. Zhuang, Y. Cai, and C. Augarde, "A meshless sub-region radial point interpolation method for accurate calculation of crack tip fields," *Theoretical and Applied Fracture Mechanics*, vol. 69, pp. 118–125, 2014.

[26] Y. Long and Y. Zhao, "Technical note: calculation of stress intensity factors in plane problems by the sub-region mixed finite element method," *Advances in Engineering Software (1978)*, vol. 7, no. 1, pp. 32–35, 1985.

[27] H. Zheng, F. Liu, and C. Li, "Primal mixed solution to unconfined seepage flow in porous media with numerical manifold method," *Applied Mathematical Modelling*, vol. 39, no. 2, pp. 794–808, 2015.

[28] M. L. Williams, "On the stress distribution at the base of a stationary crack," *Journal of Applied Mechanics*, vol. 24, no. 1, pp. 109–114, 1957.

[29] B. Karihaloo and Q. Xiao, "Linear and nonlinear fracture mechanics," *Comprehensive Structural Integrity*, vol. 2, pp. 81–212, 2003.

[30] H. Zheng, Z. Liu, and X. Ge, "Numerical manifold space of Hermitian form and application to Kirchhoff's thin plate problems," *International Journal for Numerical Methods in Engineering*, vol. 95, no. 9, pp. 721–739, 2013.

[31] P. Lancaster and K. Salkauskas, "Surfaces generated by moving least squares methods," *Mathematics of Computation*, vol. 37, no. 155, pp. 141–158, 1981.

[32] Q. Z. Xiao, B. L. Karihaloo, and X. Y. Liu, "Direct determination of SIF and higher order terms of mixed mode cracks by a hybrid crack element," *International Journal of Fracture*, vol. 125, no. 3-4, pp. 207–225, 2004.

[33] M. R. Ayatollahi and M. Nejati, "An over-deterministic method for calculation of coefficients of crack tip asymptotic field from finite element analysis," *Fatigue & Fracture of Engineering Materials & Structures*, vol. 34, no. 3, pp. 159–176, 2011.

[34] Y. K. Cheung, C. W. Woo, and Y. H. Wang, "A general method for multiple crack problems in a finite plate," *Computational Mechanics*, vol. 10, no. 5, pp. 335–343, 1992.

[35] C. Daux, N. Moës, J. Dolbow, N. Sukumar, and T. Belytschko, "Arbitrary branched and intersecting cracks with the extended finite element method," *International Journal for Numerical Methods in Engineering*, vol. 48, no. 12, pp. 1741–1760, 2000.